Bond Mechanism of NSM FRP Bars for Flexural Strengthening of Concrete Structures

Tarek K. Hassan [(1)] and Sami H. Rizkalla [(2)]

[(1)] Post-doctoral fellow, [(2)] Distinguished Professor

Department of Civil Engineering, North Carolina State University Campus Box 7533,

Raleigh, NC, USA 27695-7533

ABSTRACT

This paper presents both experimental and analytical investigations undertaken to evaluate bond characteristics of near surface mounted carbon fiber reinforced polymers (CFRP) bars. A total of eight concrete beams, strengthened with near surface mounted CFRP bars were tested under monotonic static loading. Different embedment lengths are studied to determine the development length of the FRP reinforcement. The performance of two different adhesives used to bond the bars to the surrounding concrete is examined. A general methodology to evaluate the development length of near surface mounted FRP bars of different configurations and types of fibers is presented. A quantitative criterion governing debonding failure is established. The proposed bond model assumes linear elastic behavior for the concrete, adhesive and the near surface mounted (NSM) FRP bars, following the same philosophy of the ACI provisions for bond analysis and design. The proposed analytical model is validated by comparing the predicted values to test results as well as to non-linear finite element modelling. The influence of key parameters, including the thickness of the adhesive cover, groove width, groove spacing and internal steel reinforcement configuration are discussed.

Keywords: Bond, concrete, beams, FRP, strengthening, NSM, development length

INTRODUCTION

Bond of reinforcing FRP bars, strips and sheets to concrete is a critical factor that controls the structural performance of concrete members strengthened with FRP. Up-to-date, limited research has been reported on the bond behavior of near surface mounted (NSM) FRP reinforcement. Lack of experimental data, design tools and analytical models addressing the bond characteristics of various FRP strengthening techniques introduce serious obstacles towards an efficient use of these materials. Debonding of the FRP reinforcement occurs in an abrupt manner [1-6]. Debonding failures are always brittle and are associated with a considerable reduction in the deformability of the strengthened member. Therefore, full understanding of the bond characteristics of the FRP reinforcement is crucial to the successful repair and strengthening of concrete structures.

Near surface mounting technique becomes particularly attractive for flexural strengthening in the negative moment regions of slabs and girders, where externally bonded reinforcement could be subjected to severe damage due to mechanical and environmental conditions. The initial research work on NSM technique was reported by Blaschko and Zilch (1999)[7] using CFRP strips inserted into grooves cut at the surface of concrete specimens. The specimens were tested in a double shear configuration. Test results showed that strengthening using NSM CFRP strips has a greater anchoring capacity compared to externally bonded CFRP strips. De Lorenzis and Nanni (2001)[8] investigated the structural performance of simply supported reinforced concrete beams strengthened with NSM glass and carbon FRP rods. Both flexural and shear strengthening were examined. Hassan and Rizkalla (2002)[9] investigated the feasibility of using different strengthening techniques as well as different types of FRP for flexural strengthening of large-scale prestressed concrete specimens. The specimens represented typical prestressed concrete

slab bridges. Test results showed that the use of NSM FRP bars is feasible and cost effective for strengthening concrete structures and bridges. Hassan and Rizkalla (2003)[10] investigated the bond performance of concrete structures strengthened with NSM CFRP strips. A closed-form analytical solution was proposed to predict the interfacial shear stresses and the minimum anchorage length needed to effectively use NSM FRP strips. The model was validated by comparing the predicted values with test results as well as non-linear finite element modelling. De Lorenzis and Nanni (2002)[11] examined the bond between NSM FRP bars and concrete by testing 22 unreinforced concrete beams having a span of 1067 mm and strengthened with NSM FRP bars. The influence of different parameters including the bonded length, diameter of the bars and type of FRP materials were investigated. The effect of the internal steel reinforcement configuration on the bond behavior was not demonstrated since the tested specimens were unreinforced. Moreover, the influence of the size effect using small-size specimens on the bond behavior might be significant and was not included in their proposed model. Blaschko (2003)[12] introduced an analytical model for the bond of NSM CFRP strips. The model showed that the deformations in the concrete have a strong influence on the distribution of the bond stresses and therefore on the bond capacity.

This paper presents design guidelines for an efficient use of NSM FRP bars through comprehensive experimental and analytical investigations. An analytical model is proposed to characterize the behavior of concrete structures strengthened with NSM FRP bars. The information presented in this paper is applicable to repair damaged or deteriorated concrete structures, to overcome design or structural deficiencies as well as to increase the flexural capacity of structures to accommodate higher loads beyond the original design.

RESEARCH SIGNIFICANCE

Understanding of the fundamental behavior of NSM FRP reinforcement is essential for an effective use of this technique for strengthening of concrete structures and bridges. This paper focuses on the bond characteristics of NSM FRP bars to concrete. The study provides significant contribution to the current knowledge towards durable restorative procedures of concrete structures to prevent their replacement and to ensure public safety. The study offers quantitative information regarding debonding failures and emphasizes the influence of the configuration of the original steel reinforcement on the behavior. In principle, findings of this research will enable engineers to make more informative decisions regarding the repair and/or strengthening of flexural members and will assist in developing reliable design procedures for strengthening of concrete structures and bridges with NSM FRP reinforcement.

EXPERIMENTAL PROGRAM

Test Specimens

A total of eight, simply supported T-beams with a span of 2.5 m and a depth of 300 mm, were constructed. Shear reinforcement consisted of double-legged steel stirrups (10 mm in diameter), uniformly spaced at 100 mm. The top flange was reinforced with welded wire fabric (WWF) 51x51 MW5.6 x MW5.6. The top reinforcement consisted of two 10 mm in diameter steel bars. The bottom reinforcement consisted of two 10 mm in diameter steel bars running along the full length of the beam and two 15 mm in diameter steel bars placed at 100 mm from the mid-span section of the beam on both sides as shown in Fig. 1.

This arrangement of the bottom reinforcement was selected to identify the location of flexural failure of the strengthened specimens. The yield strength and modulus of elasticity of the deformed steel bars were 400 MPa and 200 GPa, respectively as reported by the manufacturer. The T-section configuration was selected to represent typical integrated beam slab construction and to avoid compression failure due to crushing of the concrete. Selection of the specimens' dimensions was finalized after testing six pilot specimens. The performance of two different epoxy adhesives used for bonding the bars to the surrounding concrete is investigated. The specimens were adequately designed to avoid concrete crushing and premature failure due to shear.

Strengthening Procedures

One beam was tested as a control specimen, A0, while the other seven beams were strengthened with NSM CFRP bars. The bars are produced by Marshall Industries Composites Inc., USA. Based on tension tests, the bars have a modulus of elasticity of 111 GPa and an ultimate tensile strength of 1918 MPa. Three standard-size cylinders (150 mm in diameter and 300 mm in height) were tested according to the ASTM C39[13]. The average compressive strength of concrete after 28 days was 48 MPa. Each beam was strengthened using one 9.525 mm diameter CFRP bar inserted into a groove cut at the bottom surface of the beam. A special concrete saw was used to cut the grooves at the bottom surface of the beam. The groove dimensions were 18 mm wide by 30 mm deep. The epoxy was pressure injected into the grooves to cover 2/3 of the groove height. The bars were placed in the grooves and gently pressed to displace the bonding agent as shown in Fig. 2. The grooves were then filled completely with the epoxy. Quality control was achieved through continuous inspections during the installation procedures.

Beams A1, A2, A3, and A4 were strengthened with NSM CFRP bars with embedment lengths of 150, 550, 800, and 1200 mm, respectively. These beams were tested using Duralith-gel epoxy adhesive for bonding the bars to the surrounding concrete. The adhesive is produced by Tamms Industries, USA, and is commonly used as a mortar binder for vertical and overhead repairs of structural concrete. The adhesive has an average modulus of elasticity of 1200 MPa and an average tensile strength of 48 MPa as reported by the manufacturer. The embedment length, L, of the NSM CFRP bars was used on each side of the centre line of the specimen as shown in Fig. 3. To investigate the influence of the epoxy adhesive, beams A5, A6 and A7 were strengthened with NSM CFRP bars with embedment lengths of 550, 800, and 1200 mm, respectively using Kemko 040 epoxy adhesive. The adhesive is produced by ChemCo Systems, Inc., USA and is designed specifically for grouting bolts, dowels and steel rebars in concrete. The adhesive has an average modulus of elasticity of 3000 MPa and an average tensile strength of 62 MPa as reported by the manufacturer.

Test Setup and Instrumentation

The beams were tested under a concentrated load applied at mid-span. A closed-loop MTS, 1000 kN testing machine was used to apply the load using the stroke control mode. The rate of loading was 1.0 mm/min up to yielding of the internal steel reinforcement, beyond which the rate was increased to 3.0 mm/min up to failure. The instrumentation used to monitor the behavior of the beams during testing is shown in Fig. 3.

TEST RESULTS AND DISCUSSION

The load-deflection behavior of the tested specimens is shown in Figs. 4a and 4b for the two adhesives; Duralith-gel and Kemko040, respectively. The control specimen, A0, failed due to

crushing of concrete at a load level of 56 kN. Specimen A1 with an embedment length of 150 mm provided insignificant increase in stiffness or strength due to early debonding of the CFRP bar. Failure of beams A2, A3, and A4 with embedment lengths of 550, 800, and 1200 mm, respectively was due to debonding of the CFRP bar. The ultimate loads for these beams ranged between 67 kN to 79 kN, with an increase of 20 to 41 percent in comparison to the control specimen. Test results showed an identical behavior for the beams strengthened with the two sets of adhesives up to failure. Altering the type of the epoxy adhesive had a negligible effect on the ultimate load carrying capacity of the strengthened beams. It should be emphasized that both adhesives were originally used for bonding steel bars to concrete.

The observed mode of failure for all beams strengthened with NSM CFRP bars was due to splitting of the concrete surface at the concrete-epoxy interface. The observed mode of failure did not involve the internal steel reinforcement. After debonding of the NSM CFRP bars, the beams behaved as conventional concrete beams reinforced with the steel reinforcement only. The load dropped to a load level equivalent to the yielding moment of the beam and maintained until crushing of the concrete occurred at the mid-span section. Debonding occurred at the location where the secondary bottom steel reinforcements were terminated due to high shear stress concentration at this zone as shown in Fig. 5. Such a phenomenon indicates that the configuration of the original steel reinforcement significantly influences the debonding location of NSM FRP bars. Experimental results for the test specimens are summarized in Table 1.

The maximum tensile stress in NSM CFRP bars at the onset of debonding, f_{FRP}, increased by increasing the embedment length up to a length of 800 mm. Using embedment lengths greater

than 800 mm did not provide a significant increase in the maximum tensile stress in the CFRP bars. This was evident by testing specimens A4 and A7 with an embedment length of 1200 mm. Test results showed that increasing the embedment length by 50 percent resulted in an increase in the maximum tensile stress in the CFRP bars by less than 7.5 percent.

Debonding of the NSM CFRP bar took place at a very early stage for beam A1, where the bond length was set to 15 times the diameter of the bar (L=150 mm). The composite action for beam A1 was completely lost at a strain level of 0.11 percent indicating that only 6 percent of the tensile strength of the bars was utilized prior to debonding. For beams A3, A4, A6 and A7 where the bond length was set to either 80 or 120 times the diameter of the bars, the maximum measured tensile stress in the CFRP bars at the onset of debonding was almost constant and ranged from 40 to 45 percent of the tensile strength of the bars. De Lorenzis and Nanni (2002)[11] reported a limiting stress value for NSM CFRP bars of 33 percent of the tensile strength. Test results in this paper showed that such a limiting value is highly dependent on the configuration of the steel reinforcement inside the beam at the strengthened zone as well as on the stress level at the concrete-epoxy interface as will be emphasized later in this paper. Test results demonstrated that rupture of NSM CFRP bars is not likely to occur regardless of the embedment length or the type of the epoxy adhesive used. Test results suggested that the development length for NSM CFRP bars with the given groove dimensions and material properties used in this program should not be less than 80 times the diameter of the bars.

Bond Mechanisms

The slip of the NSM CFRP bars at the free end was measured and the maximum bond stresses were calculated assuming a constant stress distribution along the embedment length. The measured average bond-free-end slip relationships for NSM CFRP bars, shown in Fig. 6 suggested the following two main stages for the bond mechanism:

Stage I: represents the initial bond provided by the chemical adhesion. At this stage no slip occurs.

Stage II: represents break of the chemical adhesion and transfer of bond forces by the mechanical friction provided by the lugs of the bars. At this stage, bearing stresses in concrete and epoxy are developed and induced transverse micro cracks at the tips of the lugs allowing the bar to slip. Later in this stage, a significant increase of the bearing forces accompanied by numerous internal cracks around the deformed CFRP bars took place causing debonding failure. Debonding could occur either at the FRP-epoxy interface or at the concrete-epoxy interface[14].

Figure 6 shows that the maximum measured slip at the free end of the NSM FRP bars having an embedment length of 550 mm (beams A2 and A5) is far exceeding the free end slip values recommended by other researchers[15]. Increasing the embedment length from 550 mm to 800 mm in beams A3 and A6 decreased the maximum measured free end slip by more than 50% and provided satisfactory slip values.

ANALYTICAL MODELLING

Significance of the Model

The proposed approach presents a general methodology to evaluate the development length of NSM FRP bars of different configurations and types of fibers. The model is based on equilibrium and displacement compatibility procedures using finite element analysis. The ACI approach used to evaluate the development length of steel bars was selected as a starting point for the proposed approach. The model accounts for distinct characteristics of concrete, epoxy and FRP materials. A design chart for calculating the development length of NSM FRP bars is proposed. The influence of various parameters including the groove width, adhesive cover, and material properties is discussed.

Proposed Approach

The philosophy of the proposed approach is to provide rules to preclude significant amounts of plasticity in the concrete and adhesive surrounding a NSM FRP bar. Within this range of response, detailed bond plasticity models are not essential and an assumed constant bond stress distribution along the anchorage length is acceptable. In the proposed approach, transfer of stresses from a deformed NSM FRP rod to the concrete is assumed to be mainly through the mechanical interlocking of the lugs to the surrounding adhesive. Due to the shape of the lugs, the resultant force exerted by the lug to the adhesive is inclined by an angle β with respect to the axis of the bar as shown in Fig. 7, where 1/tan β is the coefficient of friction, μ, between the bar and the adhesive.

The radial component of the resultant force creates zones of high tensile stresses at the FRP-adhesive interface as well as at the concrete-adhesive interface. Thick-walled cylinder theory has been applied by many researchers to analyze the stresses in a concrete cylinder surrounding a single bar[16-17]. Lack of confinement, uneven distribution of bond stresses, edge effects and composite interaction between concrete, adhesive and FRP materials complicate the analysis of NSM FRP bars. Consequently, thick-walled cylinder theory may not apply in this case.

The proposed approach is based on 2-D finite element analysis to provide fundamental understanding of the bond characteristics and load transfer mechanism between NSM FRP bars and concrete. The finite element modelling described in this paper was conducted using ADINA program (Version 7.4). Fig. 8 shows the mesh dimensions used in modelling a portion of a concrete beam strengthened with a NSM FRP bar using epoxy as an adhesive. The concrete and the epoxy were modelled using eight-node plain strain elements with a 3x3 Gauss integration scheme. Groove dimensions, bar location and properties of concrete and epoxy were set identical to those used in the test specimens. Radial pressure was applied at the bar location to simulate the bond stresses transferred from the bar to the surrounding epoxy. The maximum tensile stress components in the two global orthogonal axes, Y-Y and Z-Z axes are shown in Fig. 9.

It should be noted that the elastic modulus of the adhesive is generally less than that of the concrete. Such a phenomenon results in a stress discontinuity at the concrete-epoxy interface as shown in Fig. 9. High tensile stresses are observed at the concrete-epoxy interface as well as at the FRP-epoxy interface. Two different types of debonding failures can occur for NSM FRP bars. The first mode of failure is due to splitting of the epoxy cover as a result of high tensile

stresses at the FRP-epoxy interface, and is termed "epoxy split failure". Increasing the thickness of the epoxy cover reduces the induced tensile stresses significantly. Furthermore, using adhesives of high tensile strength delays epoxy split failure. These findings explain the observed mode of failure by De Lorenzis and Nanni (2001)[8]. Epoxy split failure usually forms with longitudinal cracking through the epoxy cover. The second mode of failure is due to cracking of the concrete surrounding the epoxy adhesive and is termed "concrete split failure". This mode of failure takes place when the tensile stresses at the concrete-epoxy interface reach the tensile strength of the concrete. Widening the groove minimizes the induced tensile stresses at the concrete-epoxy interface and increases the debonding loads of NSM bars. Concrete split failure was the governing mode of failure for the test specimens reported in this investigation. Large epoxy cover and high tensile strength of the epoxy adhesive provided high resistance to epoxy split failure and shifted the failure to occur at the concrete-epoxy interface[14].

Flexural analysis indicates that the tensile stress along the length of the NSM CFRP bar increases linearly by moving away from the supports towards the applied load up to certain zone close to the mid-span section. Curtailment of the internal steel reinforcement near mid span changes the tensile force distribution in the NSM CFRP bar and increases the bond stress significantly at this zone as will be illustrated by non-linear finite element analysis later in this paper. Transfer of the tensile forces from the curtailed steel reinforcement to the continuous steel and CFRP bars is a complicated process that takes place over a certain zone and depends on the level of the tensile stresses in the continuous steel bars. The tensile strain distribution along the NSM CFRP bar is shown in Fig. 10 for beams A3 and A6. It is clear from Fig. 10 that the tensile strain distribution

can be approximated to follow a linear distribution along the length of the NSM CFRP bar[18-19]. Therefore, the tangential bond stress, τ, can be estimated with an average value of:

$$\tau = \frac{d}{4}\frac{f_{FRP}}{L_d} \tag{1}$$

where d is the diameter of the bar, and L_d is the embedment length needed to develop a stress of f_{FRP} in the NSM bar. If the coefficient of friction between the bar and the epoxy is μ, the radial stresses, σ_{radial}, shown in Fig. 7 can be expressed as:

$$\sigma_{radial} = \frac{\tau}{\mu} = \frac{d}{4}\frac{f_{FRP}}{\mu L_d} \tag{2}$$

The tensile stresses at the concrete-epoxy interface, $\sigma_{con\text{-}epoxy}$, and at the FRP-epoxy interface, $\sigma_{FRP\text{-}epoxy}$, shown in Fig. 9, can be expressed in terms of the radial stress as follows:

$$\sigma_{con-epoxy} = G_1 \frac{d}{4}\frac{f_{FRP}}{\mu L_d} \tag{3}$$

$$\sigma_{FRP-epoxy} = G_2 \text{ or } G'_2\left[\frac{d}{4}\frac{f_{FRP}}{\mu L_d}\right] \tag{4}$$

where G_1, G_2 and G'_2 are coefficients, determined from the finite element analysis based on a unit radial pressure applied at the bar location and using specified groove dimensions, concrete and adhesive properties. The maximum tensile stresses at the FRP-epoxy interface, $\sigma_{FRP\text{-}epoxy}$, depends on the coefficients G_2 and G'_2, whichever is greater as shown in Fig. 9. Equating the tensile strength of concrete to Eq. (3), the minimum embedment length needed for NSM FRP bars to prevent concrete split failure can be expressed as:

$$L_d = G_1 \frac{d}{4}\frac{f_{FRP}}{\mu f_{ct}} \tag{5}$$

Equating the tensile strength of the adhesive to Eq. (4), the minimum embedment length needed for NSM FRP bars to avoid epoxy split failure shall not be less than:

$$L_d = G_2 \ or \ G'_2 \left[\frac{d}{4} \frac{f_{FRP}}{\mu f_a} \right] \tag{6}$$

where f_{ct} and f_a are the tensile strength of concrete and adhesive, respectively. Increasing the stiffness of concrete by using high strength concrete, increases the tensile stresses at the concrete-epoxy interface. Furthermore, increasing the stiffness of the adhesive increases the tensile stresses at the FRP-epoxy interface. The modular ratio, n, can be defined as:

$$n = \frac{E_c}{E_a} \tag{7}$$

where E_c and E_a are the modulus of elasticity of concrete and adhesive, respectively. Practical values of the modular ratio, n, can vary between 5 and 40. This range covers various types of concrete and adhesives that are commonly used in concrete structures. Fig. 11 shows a proposed design chart for the development length of NSM FRP bars. To simulate the most critical conditions for design purposes, the coefficient G_1 was evaluated for a modular ratio of 40, which represents the case of high strength concrete and low stiffness adhesive. The coefficients, G_2 and G'_2 were evaluated for a modular ratio of 5 to simulate cases of low strength concrete and high stiffness adhesive. The curves represent the greater of the two coefficients G_2 and G'_2. The chart covers a wide range of possible epoxy covers, C/d, and accounts for three different groove sizes, w.

The chart clearly indicates that increasing the thickness of the epoxy cover, C/d, reduces the tensile stresses in both the concrete and the adhesive as is evident by the reduction of G_1, G_2 and G'_2 with the increase of C/d. Furthermore, using wider grooves, w, increases the tensile stresses

at the FRP-epoxy interface (G_2 and/or G'_2) due to the substantial increase in the area of adhesive and consequently in its stiffness. Using the proposed design chart, the coefficients G_1 and the greater value of either G_2 or G'_2 could be evaluated for a given groove width, w, and using a specified clear cover to the bar diameter ratio (C/d). The governing development length for NSM FRP bars could be predicted using the greater of Eq. (5) and Eq. (6). The coefficient of friction between CFRP bars and different epoxy adhesives used in this study to bond the NSM bars to the concrete was determined according to the ASTM, G115-98[20]. Smooth- and rough-surface topographies of the adhesives were tested. The rough-surface topography of the adhesives was accomplished by printing the lugs' pattern of the CFRP bars in the adhesive prior to hardening. Each set of tests were repeated twelve times. Test results showed that the average coefficients of friction between CFRP bars and adhesives of rough- and smooth-surface topographies were 0.66 and 0.33, respectively with an average value of 0.5.

Verification of the Proposed Model

Using the proposed design chart in Fig. 11 with a groove width equals to twice the diameter of the bar ($w=2d$), and a clear cover to bar diameter ratio of one (C/d=1.0), the coefficients G_1 and the greater of G_2 and G'_2 for the bond specimens reported in this investigation are 0.65 and 1.1, respectively. The diameter of the bar is 9.525 mm. The average tensile strength of the concrete used in the test specimens is 4.3 MPa. Using Eq. (5) and Eq. (6), the minimum embedment length needed to develop 40 percent of the ultimate strength of the bars, as measured by the experimental program, shall not be less than 834 mm, which is consistent with the measured value of 800 mm. The limiting value of the 40 percent of the tensile strength of NSM CFRP bars can be predicted in light of the discussion provided later in this paper.

Comparison with ACI—440

The ACI 440.1R-01[21] suggests the following expression for the development length, L_d, to avoid splitting failures in concrete structures reinforced with FRP bars:

$$L_d = 0.028 \frac{\pi d^2 f_u}{4\sqrt{f'_c}} \quad (8)$$

where, d is the diameter of the bar; f_u is the tensile strength of the bar and f'_c is the concrete compressive strength after 28 days. Using the stress limit of 40 percent of the tensile strength of the CFRP bars as observed by the experimental program, d=9.525 mm, f'_c =48 MPa, the embedment length needed to develop a stress of 40 percent of the rupture strength of the CFRP bars according to Eq. (8), is equal to 221 mm. This value is equivalent to 28 percent of the value measured when the same bars were used for strengthening the beam in a NSM configuration. The results suggest that the ACI expression is not adequate for NSM FRP bars. The significant discrepancy could be attributed to the following reasons:

a) The ACI expression is developed to characterize the bond of FRP bars to concrete. In NSM FRP bars, the bond is primarily governed by the surface characteristics of the adhesive, which is considerably smoother than concrete and requires longer development length to achieve the same bond stress compared to concrete.

b) The ACI expression assumes a coefficient of friction between FRP bars and concrete equals to 1.0. This value is typically used for steel bars bonded to concrete and has been confirmed by many researchers[22]. The coefficient of friction between FRP bars and epoxy is lower and ranges between 30 to 60 percent of the value used by the ACI. Consequently, longer development length is needed for NSM FRP bars.

c) The ACI-expression is designed for concrete structures reinforced with FRP bars where large concrete covers are typically used. For NSM FRP bars, the thickness of the epoxy cover is greatly influenced by the location of the internal steel reinforcement. Therefore, the thickness of the epoxy covers are always limited. This type of configuration induces higher tensile stresses at both the concrete-epoxy and the FRP-epoxy interface and consequently requires longer development length.

d) The ACI expression assumes full confinement of FRP bars by steel and/or FRP stirrups. Lack of such confinement in NSM FRP bars results in higher bond stresses and consequently longer development length is needed.

Therefore, it can be concluded that the *C/d* ratio and the groove width, *w*, affect the development length for NSM FRP bars and should be considered in future design guidelines.

Influence of Groove Spacing, Groove Size and Edge Distance

Closely spaced arrangement of NSM bars could magnify the tensile stresses at the concrete-epoxy interface and expedite concrete split failure. In this section, the finite element model was used to investigate the influence of clear groove spacing, *s*, as well as edge distance, *e* on interfacial stresses. The clear spacing between the grooves of NSM bars was varied from 0.25*d* to 2.0*d*, where *d* is the diameter of the bar. The groove width was also varied from 1.5*d* to 2.5*d* to examine its effect on the induced stresses.

The analysis indicates that the tensile stress at the concrete-epoxy interface is greatly influenced by the clear spacing between the grooves of NSM FRP bars. Increasing the clear groove spacing to bar diameter ratio reduces the tensile stress considerably up to a clear groove spacing of 2.0*d*,

where d is the diameter of the bars. Increasing the clear groove spacing beyond this limit has a negligible effect on the induced tensile stresses as shown in Fig. 12a. The limiting value of the clear spacing of $2d$ is independent on the groove width. The analysis indicates also that the clear spacing between the grooves of NSM bars has a negligible effect on the induced tensile stresses at the FRP-epoxy interface. These stresses are greatly influenced by the groove width rather than the clear spacing between the grooves. The analysis suggests that the minimum clear spacing between the grooves of NSM FRP bars should not be less that twice the diameter of the bars regardless of the groove width. Using clear groove spacing to bar diameter ratio less than the proposed value results in overlapping of the tensile stresses at the concrete-epoxy interface and accelerates debonding failure.

To determine the minimum edge distance required for NSM FRP bars, the edge distance, e, was varied from $2d$ to $6d$, where d is the diameter of the bar. The maximum tensile stress at the concrete-epoxy interface due to a unit radial pressure applied at the location of the FRP bars (coefficient G_1) is shown in Fig. 12b for various edge distances. In general, increasing the edge distance reduces the induced tensile stresses considerably regardless of the groove width. The analysis suggests a minimum edge distance of four times the diameter of the bars to minimize the "edge effect" and permit using the proposed design chart, shown in Fig. 11.

Maximum Tensile Stresses in NSM FRP Bars (f_{FRP})

Test results showed that the maximum tensile stress in NSM CFRP bars at the onset of debonding did not exceed 40 to 45 percent of the tensile strength of the bars regardless of the embedment length used. Initiation of the debonding failure was observed at the concrete section

where the secondary bottom steel reinforcement was terminated. This section investigates the influence of various configurations of the bottom steel reinforcement on the behavior based on a non-linear finite element modelling. Termination of the bottom steel reinforcement in the maximum moment region simulates cases where the bottom steel reinforcement is corroded or damaged. Consequently, evaluation of the existing concrete structures and identifying the conditions as well as the configuration of the internal steel reinforcement is essential prior to strengthening using NSM FRP bars. Taking advantage of the symmetry of the bond specimens, only one quarter of the beams was modelled by ANACAP using 20-node brick elements. The ANACAP software employs the classical incremental theory of plasticity that relates the increment of plastic strain to the state of stresses and stress increment. Formulation of the yield surfaces, loading, and failure surfaces take into account the effect of confinement on the concrete behavior. The concrete material is modelled by the smeared cracking methodology in which progressive cracking is assumed to be distributed over an entire element[23]. The reinforcing rebars were modeled as individual sub-elements within the concrete brick elements. The stiffness and strength contributions of the reinforcing rebar are calculated by integrating along the rebar and distributing over the concrete elements through the associated shape functions. This methodology is consistent with the smeared cracking philosophy for concrete modeling. Verification of the ANACAP program using independent experimental results can be found elsewhere [9, 24]. In the analysis, the embedment length of NSM CFRP bars was set to 550 mm to develop the maximum bond stresses as observed in the experimental program for beams A2 and A5. Four different configurations for the bottom steel reinforcement were examined as shown in Fig. 13. Using Eq. (1) and Eq. (5) and rearranging, the bond strength of NSM FRP bars, τ_{max}, can be expressed as:

$$\tau_{\max} = \frac{\mu f_{ct}}{G_1} \tag{9}$$

where μ is the coefficient of friction between FRP bars and bonding adhesives; f_{ct} is the tensile strength of concrete and G_1 is a coefficient determined using the proposed design chart given in Fig. 11 for specified groove dimensions. Using an average coefficient of friction between CFRP bars and the adhesive of 0.5, tensile strength of concrete of 4.3 MPa and G_1 of 0.65 for the bond specimens reported in this investigation, the bond strength was calculated and is equal to 3.3 MPa, which is 10 percent higher than the measured value, reported in Table 1. Eq. (9) was adopted in the finite element analysis as a criterion for debonding failure at the concrete-epoxy interface. The numerical simulations were conducted using a typical steel reinforcement ratio of flexural members of 1.0 percent.

Typical interfacial shear stress distribution, at failure, is shown in Fig. 14. In general, terminating bottom steel reinforcement at the maximum moment region creates zones of high bond stresses and therefore, accelerates debonding failure. Equilibrium and compatibility provisions require full transmission of the tensile stresses in the terminated steel bars to neighbouring steel and FRP bars. These tensile forces are distributed to the neighbouring bars according to their axial stiffnesses and create additional bond stresses in the steel and FRP bars. Such a phenomenon becomes more severe after yielding of the main steel reinforcement. At this stage, NSM CFRP bars receive the full tensile stresses and extremely high bond stresses are developed resulting in splitting-type failures. Therefore, doubling the area of the main steel reinforcing bars has no effect on the maximum tensile stresses in NSM CFRP bars at the onset of debonding. This behavior was confirmed through a set of numerical simulations using a steel reinforcement ratio of 2.0 percent at the mid-span section.

The analysis indicated that terminating 10 percent of the main bottom steel reinforcement allowed the CFRP bars to utilize 60 percent of its tensile strength prior to debonding. It should be noted that terminating 50 percent or more of the main bottom steel reinforcement induce high bond stresses and limit the tensile stresses at the onset of debonding of NSM CFRP bars to 40 percent of the tensile strength of the bars. The results of the analysis coincided with the measured values in the experimental program.

Based on the reported experimental and analytical investigations, typical procedures to evaluate the development length of any configuration of NSM FRP bars can be summarized as follows:

a) Determine the material characteristics of FRP bars, concrete and adhesive.
b) Determine the coefficient of friction between the FRP bar and the bonding adhesive according to the ASTM G115-98[20] or based on information provided by the manufacturer.
c) Select groove dimensions, thickness of the clear epoxy cover and use the proposed design chart, given in Fig. 11 to determine the coefficients G_1 and the greater of coefficients G_2 and/or G'_2.
d) Determine the maximum allowable tensile stress in NSM CFRP bars prior to debonding using either non-linear finite element analysis or laboratory testing. A conservative value of 40% of the tensile strength of the CFRP bars can be used alternatively.
e) Calculate the development length using the greater of Eq. (5) and Eq. (6)
f) Reselect groove dimensions if necessary and repeat steps (c) to (e).

CONCLUSIONS

Based on the findings of this investigation, the following conclusions can be drawn:

1. The use of NSM CFRP bars is feasible and effective for strengthening/repair of concrete structures. The technique can be used to increase both stiffness and flexural strength of concrete beams.
2. The development length of NSM FRP reinforcement is highly dependent on the dimensions of the bars, concrete and adhesive properties, reinforcement configuration, and groove width. Consequently, complete evaluation of the existing structures is compulsory prior to any strengthening application.
3. Rupture of NSM CFRP bars is not likely to occur regardless of the embedment length used. The efficiency of using CFRP bars as NSM reinforcement is controlled primarily by the bond characteristics of the bars as well as by the bond between the adhesive material and the concrete.
4. The development length of NSM CFRP bars tested in this investigation should not be less than 80 times the diameter of the bars.
5. The maximum measured tensile strain in the CFRP bars at failure is in the range of 40 to 45 percent of the rupture strain of bars, regardless of the embedment length used. Such a limiting value is highly dependent on the configuration of the bottom steel reinforcement inside the beam as well as on the stress level at the concrete-epoxy interface.
6. The proposed design chart is adequate to determine the development length of NSM FRP bars accurately. The chart is easy to use and provides excellent correlation to experimental results.

7. Two different types of debonding failures can occur for NSM FRP bars. The first mode of failure is due to splitting of the epoxy cover as a result of high tensile stresses at the FRP-epoxy interface, and is termed “epoxy split failure”. The second mode of failure is due to cracking of the concrete surrounding the epoxy adhesive and is termed “concrete split failure”.
8. Increasing the groove width and/or using high strength concrete, increases the resistance to concrete split failure. Using high strength adhesives and/or increasing the epoxy cover layer delays epoxy split failure for NSM FRP bars.
9. The proposed minimum clear spacing between the grooves of NSM FRP bars is twice the diameter of the bars regardless of the groove width. A minimum edge distance of four times the diameter of the bars is recommended to diminish edge effect for NSM FRP bars.
10. Termination or damage of the internal steel reinforcement creates zones of high bond stresses and accelerates debonding failure. Increasing the reinforcement ratio of the terminated and/or damaged steel reinforcement results in a proportional increase in the bond stress and a corresponding decrease in debonding loads.

ACKNOWLEDGMENTS

The authors wish to acknowledge the support of the Network of Centres of Excellence, ISIS Canada, program of the Government of Canada and the Natural Science and Engineering Research Council. The writers gratefully acknowledge the support provided by Marshall Industries Composites Ltd, United States for providing the materials used in the test program. The authors would like also to acknowledge the support provided by Concrete Restoration Inc.,

Winnipeg, Canada for performing all the strengthening work. Special thanks to M. McVey for his assistance during fabrication and testing of the specimens.

NOTATION

C = adhesive cover

d = diameter of NSM FRP bar

e = edge distance for NSM FRP bars

E_a = modulus of elasticity of the adhesive

E_c = modulus of elasticity of concrete

f_{ct} = tensile strength of concrete

f_a = tensile strength of adhesive

f_{FRP} = maximum tensile stress in NSM FRP bars at the onset of debonding

f_u = tensile strength of CFRP bars

$G_{1,2,2'}$ = coefficients for NSM FRP bars

L_d = development length of NSM CFRP bars

n = modular ratio

P_u = failure load

s = clear spacing between grooves

w = groove width

β = angle of inclination of bond stresses to the bar axis

δ = slip at free end

Δ_u = deflection at mid-span section at failure

ε_d = maximum tensile strain of the CFRP reinforcement at debonding failure

μ = coefficient of friction between NSM FRP bars and adhesives

$\sigma_{con\text{-}epoxy}$ = tensile stress at the concrete-epoxy interface

$\sigma_{FRP\text{-}epoxy}$ = tensile stress at the FRP-epoxy interface

σ_{radial} = radial stress on a NSM FRP bar

τ = average bond stress

τ_f = average bond stress at failure

τ_{max} = bond strength

REFERENCES

1. Saadatmanseh, E., and Ehsani, M. R. "Application of Fibre-Composites in Civil Engineering." *Proceedings of the 7th ASCE Structures Congress*, 1989, pp. 526-535.
2. Meier, U., and Kaiser, H.P. "Strengthening of Structures with CFRP Laminates, Advanced Composite Materials in Civil Engineering Structures." *ASCE Specialty Conference*, 1991, 224-232.
3. Ritchie, P.A., Thomas, D.A., Lu, L., and Connelly, G.M. "External Reinforcement of Concrete Beams Using Fibre Reinforced Plastics." *ACI Structural Journal*, V. 88, No. 4, 1991, pp. 490-500.
4. Sharif, A., Al-Sulaimani, G. J., Basunbul, I. A., Baluch, M.H., and Ghaleb, B.N. "Strengthening of Initially Loaded Reinforced Concrete Beams Using FRP Plates." *ACI Structural Journal*, V. 91, No. 2, 1994, pp. 160-168.
5. Arduini, M., Di Tommaso, A., and Nanni, A. "Parametric Study of Beams with Externally Bonded FRP Reinforcement." *ACI Structural Journal*, V. 94, No. 5, 1997, pp. 493-501.
6. Karbhari, V.M., Engineer, M., and Eckel, D.A. "On the Durability of Composite Rehabilitation Schemes for Concrete: Use of a Peel Test." *Journal of Material Science,* V. 32, No. 1, 1997, pp. 147-156.

7. Blaschko, M., and Zilch, K. “Rehabilitation of Concrete Structures with Strips Glued into Slits.” *Proceedings of the 12th Int. Conference on Composite Materials*, Paris, 1999, CD-Rom.
8. De Lorenzis L., and Nanni, A. “Shear Strengthening of Reinforced Concrete Beams with Near-Surface Mounted Fibre Reinforced Polymer Rods.” *ACI Structural Journal,* V. 98, No. 1, 2001, pp. 60-68.
9. Hassan, T., and Rizkalla, S. “Flexural Strengthening of Prestressed Bridge Slabs with FRP Systems.” *PCI Journal,* V. 47, No. 1, 2002, pp. 76-93.
10. Hassan, T., and Rizkalla, S. “Investigation of Bond in Concrete Structures Strengthened with NSM CFRP strips” *Journal of Composites for Construction*, V. 7, No. 3, 2003, pp. 248-257.
11. De Lorenzis L. and Nanni, A. “A. Bond Between Near-Surface Mounted FRP Rods and Concrete in Structural Strengthening”, *ACI Structural Journal*, V. 99, No. 2, 2002, pp. 123-132.
12. Blaschko, M., “Bond Behavior of CFRP Strips Glued into Slits” Proceedings of the sixth International Conference Symposium on FRP Reinforcement for Concrete Structures (FRPRCS-6), Singapore 2003, Vol. 1, pp. 205-214.
13. ASTM C-39-01 “Standard Test Method for Compressive Strength of Cylinderical Concrete Specimens” Annual Book of ASTM Standards, Vol. 04.02.
14. Rizkalla, S. and Hassan, T. “Effectiveness of FRP Techniques for Strengthening Concrete Structures”, *Journal of the International Association of Bridges and Structural Engineering*, 2002, V.12, No. 2, pp. 89-95.

15. Mathey, R.G., and Watstein, D.“Investigation of Bond in Beam Pull-out Specimens with High Yield Strength Deformed Bars”, *ACI Structural Journal*, 1961, V. 57, No. 9, pp.1071-1090.
16. Orangun, C.O., Jirsa, J.O., and Breen, J.E. “A Reevaluation of Test Data on Development Length and Splices”, *ACI Structural Journal*, V. 74, No. 3, 1977, pp.114-122.
17. Mahmoud, Z., Rizkalla, S.H., and Zahgloul, E. “Transfer and Development Lengths of Carbon Fibre Reinforced Polymers Prestressing Reinforcement” *ACI Structural Journal*, V. 96, No. 4, 1999.
18. Nguyen, D. M., Chan, T. K. and Cheong, H., K., **“**Brittle Failure and Bond Development Length of CFRP-Concrete Beams” 2001, *ASCE Journal of Composites for Construction*, V. 5, No. 1, pp. 12-17.
19. Fanning, P. J. and Kelly, O., “Ultimate Response of RC Beams Strengthened with CFRP Plates”, 2001, *ASCE Journal of Composites for Construction*, V. 5, No. 2, pp. 122-127.
20. ASTM G115-98 “Standard Guide for Measuring and Reporting Friction Coefficients” Annual Book of ASTM Standards, Vol. 15.01.
21. ACI 440.1R-01 “Guide for the Design and Construction of Concrete Reinforced with FRP Bars” *American Concrete Institute*, 2001, Framington Hills, Michigan, USA.
22. Goto, Y. “Cracks Formed in Concrete Around Deformed Tension Bars” *ACI Structural Journal*, V. 68, No. 4, 1971, pp. 244-251.
23. Gerstle, K. H. “Material Modelling of Reinforced Concrete”, *IABSE Colloquium on Advanced Mechanics of Reinforced Concrete, Introductory Report*, Delft, 1981.
24. Hassan, T., Abdelrahman, A., Tadros, G., and Rizkalla, S. “ FRP Reinforcing Bars For Bridge Decks” *Canadian Journal for Civil Engineering*, V. 27, No. 5, 2000, pp. 839-849.

Table 1 Summary of test results

Beam No.	L (mm)	Epoxy used	P_u (kN)	Δ_u (mm)	ε_d (%)	f_{FRP} (MPa)	f_{FRP}/f_u (%)	τ_f (MPa)	Failure mode
A0	N.A	N.A	56	64	-	-	-	-	C [+]
A1	150	Duralith-gel	56	78	0.11	122	6.4	1.93	D [*]
A2	550		67	15.3	0.63	699	36.4	3.0	D
A3	800		73	21.2	0.73	810	42.2	2.40	D
A4	1200		79	24.2	0.78	866	45	1.72	D
A5	550	Kemko 040	59	12	0.60	666	34.7	2.9	D
A6	800		70	16.5	0.68	755	39.3	2.3	D
A7	1200		76	25.8	0.73	810	42.2	1.61	D

[+] C refers to crushing of concrete and steel yielding

[*] D refers to debonding of CFRP bars.

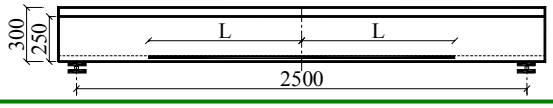

where L is the bond length; P_u is the ultimate failure load; Δ_u is the deflection at failure; ε_d is the maximum tensile strain in CFRP bars at debonding failure; f_{FRP} is the maximum tensile stress in CFRP bars at debonding failure; f_u is the tensile strength of CFRP bars (1918 MPa); and τ_f is the average bond stress at failure.

List of Figures

Biographical Sketch of the Authors

ACI member **Tarek K. Hassan** *is a postdoctoral research associate at North Carolina State University. He received his BSc from Ain-Shams University, Cairo, Egypt, and his MSc and PhD from the University of Manitoba, Canada in 1999 and 2002, respectively. His research interests include applications of fiber-reinforced polymers for repair and strengthening of concrete structures and finite element analysis of concrete structures and bridges.*

Sami H. Rizkalla, *FACI, is Distinguished Professor of Civil Engineering and Construction and Director of the Constructed Facilities Laboratory (CFL) at North Carolina State University. He is a member of the ACI Committee 440, Fiber Reinforced Polymer Reinforcement, and is a member of Joint ACI-ASCE Committee 550, Precast Concrete Structures.*

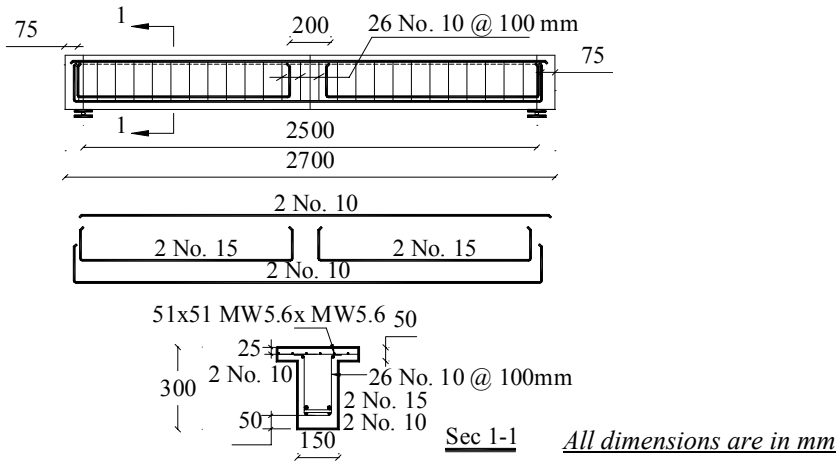

Fig. 1 Reinforcement details of test specimens

i-cutting the groove

ii-filling the groove with epoxy

iii-inserting the bar inside the groove

Fig. 2 Strengthening procedures for test specimens

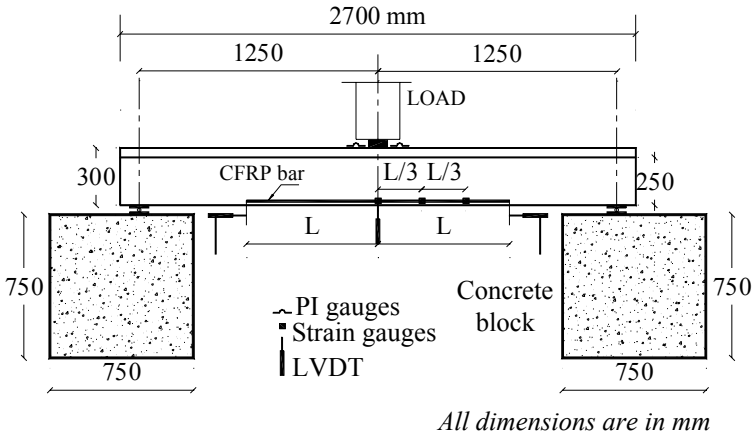

All dimensions are in mm

Fig. 3 Instrumentation used for test specimens

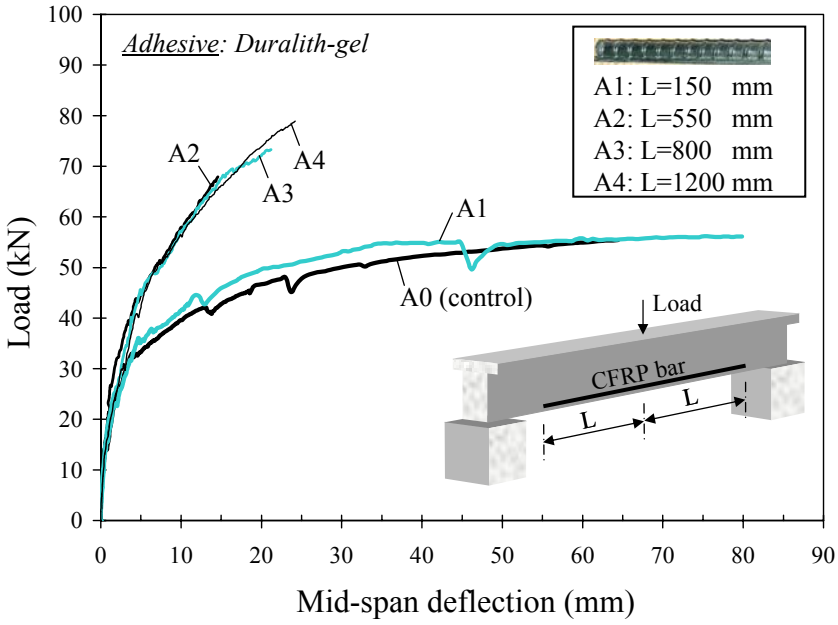

Fig. 4a Load-deflection behavior of test specimens using Duralith-gel as the bonding adhesive

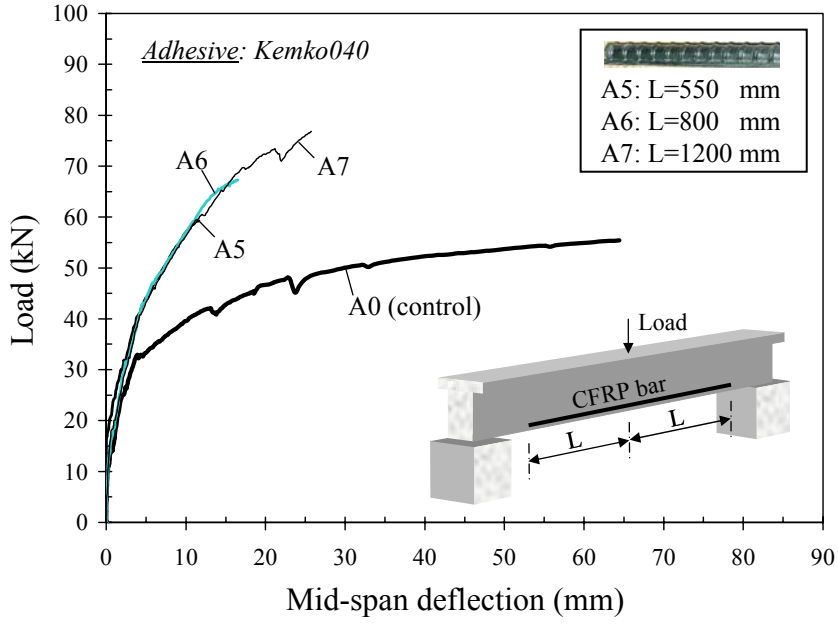

Fig. 4b Load-deflection behavior of test specimens using Kemko040 as the bonding adhesive

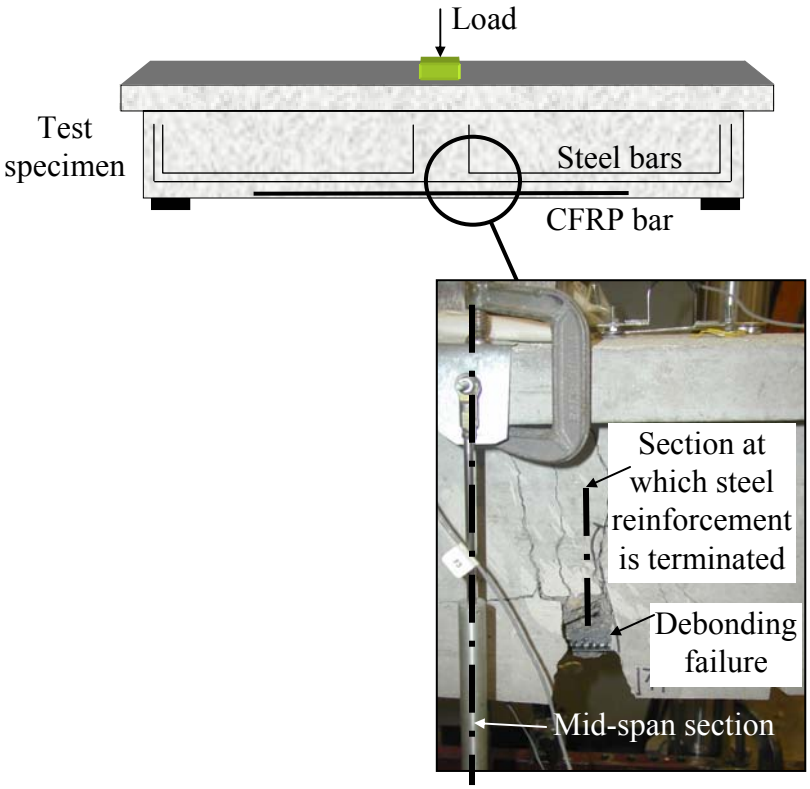

Fig. 5 Debonding of NSM CFRP bars

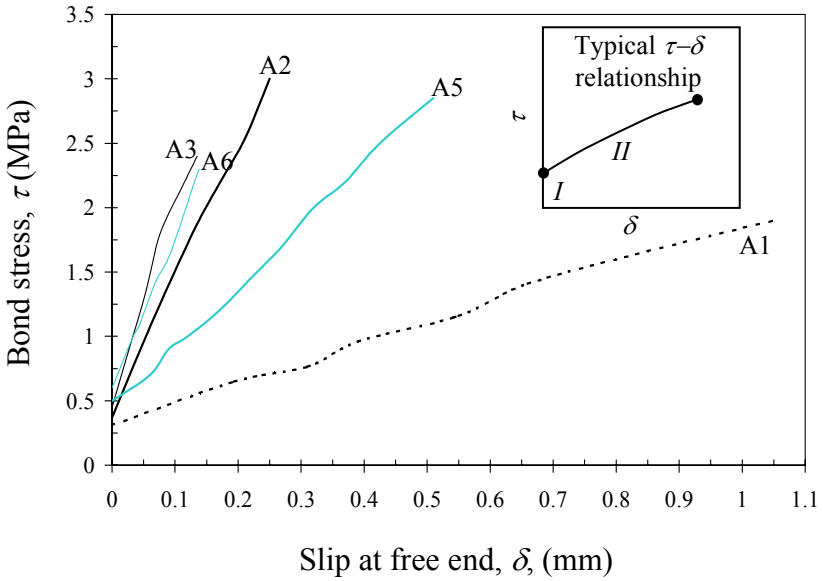

Fig. 6 Bond-slip relationship for NSM CFRP bars

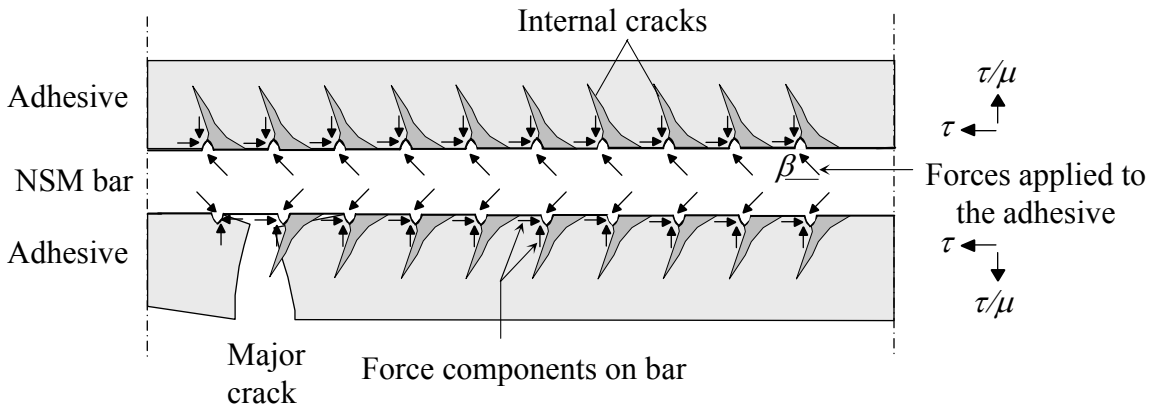

Fig. 7 Forces between a NSM FRP bar and adhesive

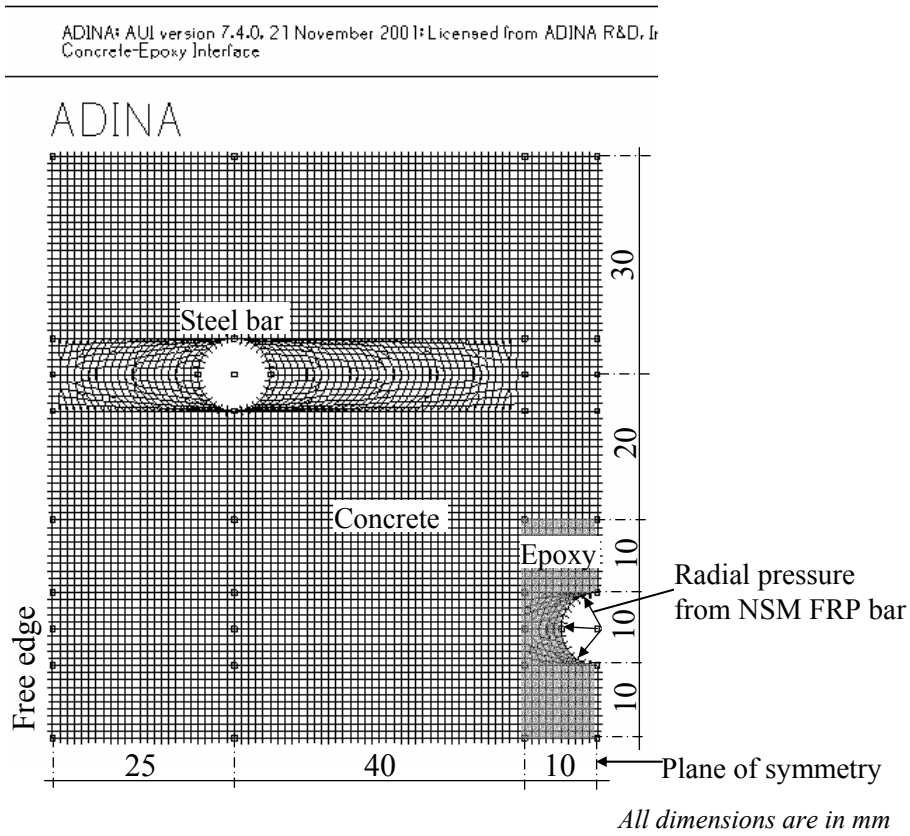

Fig. 8 Mesh dimensions for a portion of a concrete beam strengthened with a NSM FRP bar

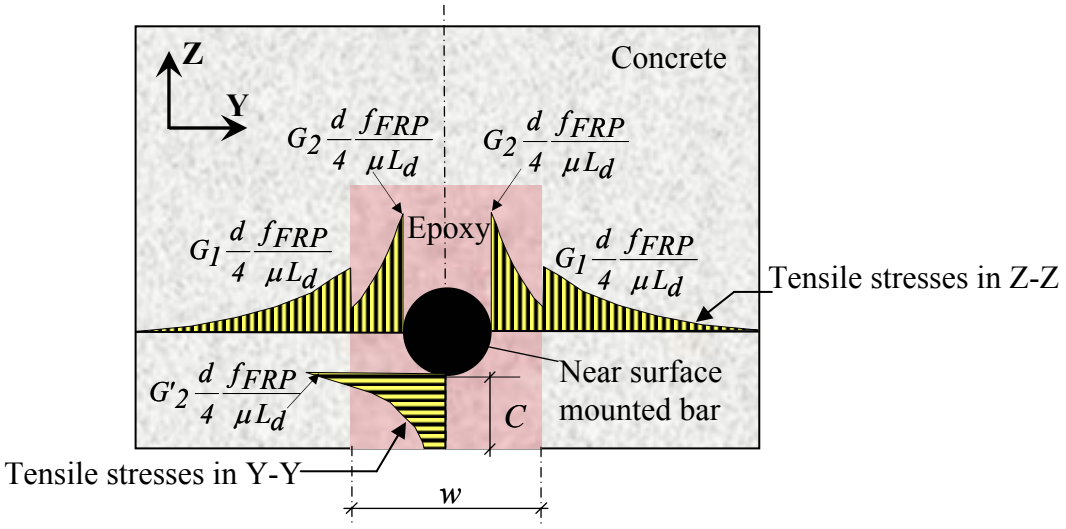

Fig. 9 Typical stress distribution around a NSM bar

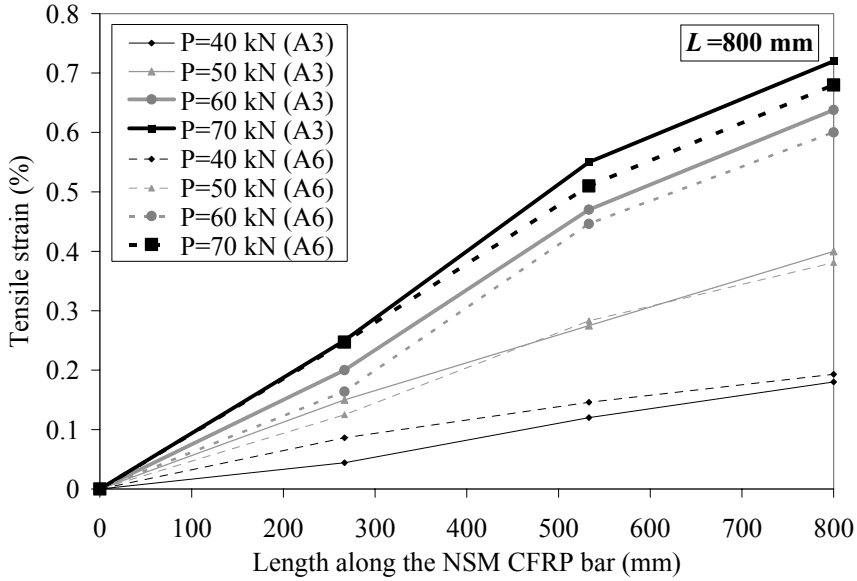

Fig. 10 Tensile strain distribution along the length of the NSM CFRP bars

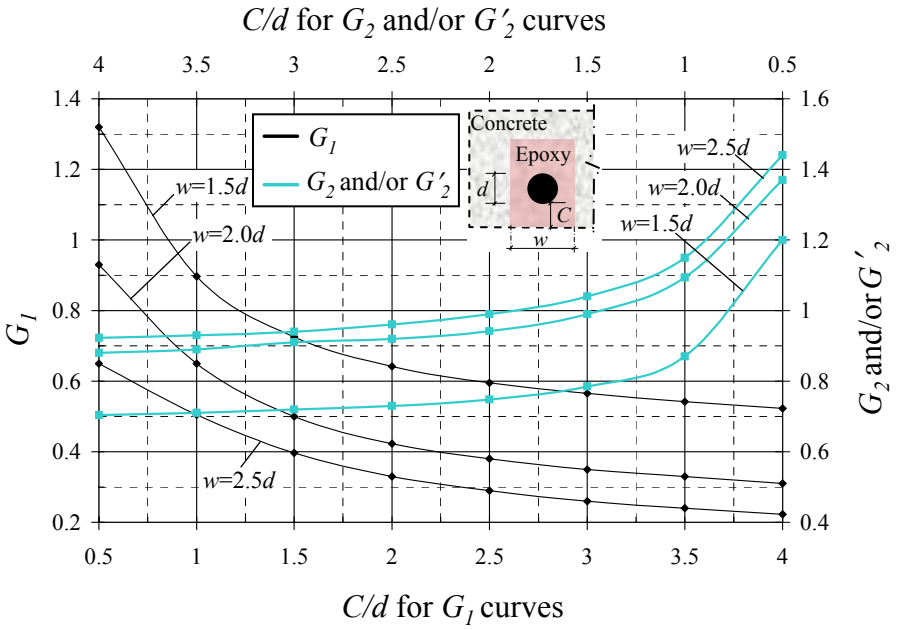

Fig. 11 Design chart for the development length of NSM FRP bars

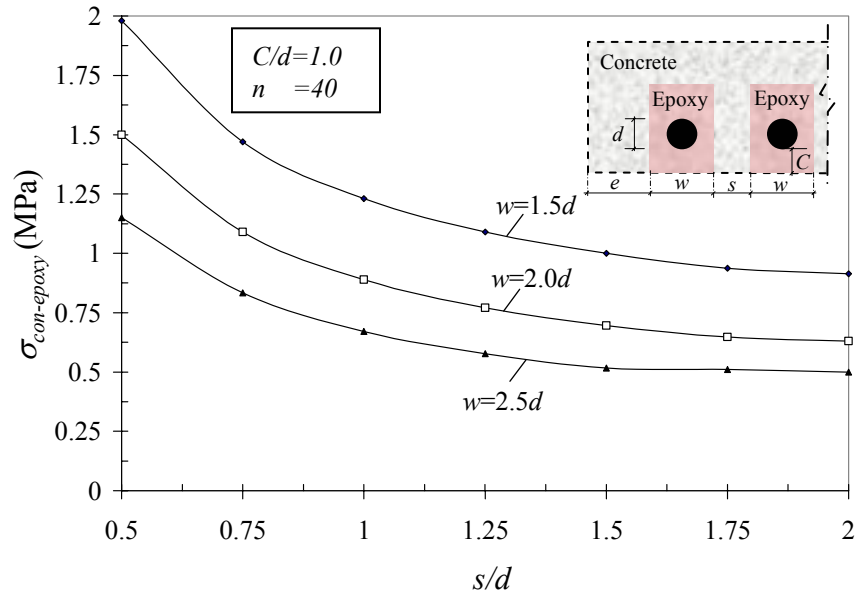

Fig. 12a Influence of groove spacing on tensile stresses at the concrete-epoxy interface

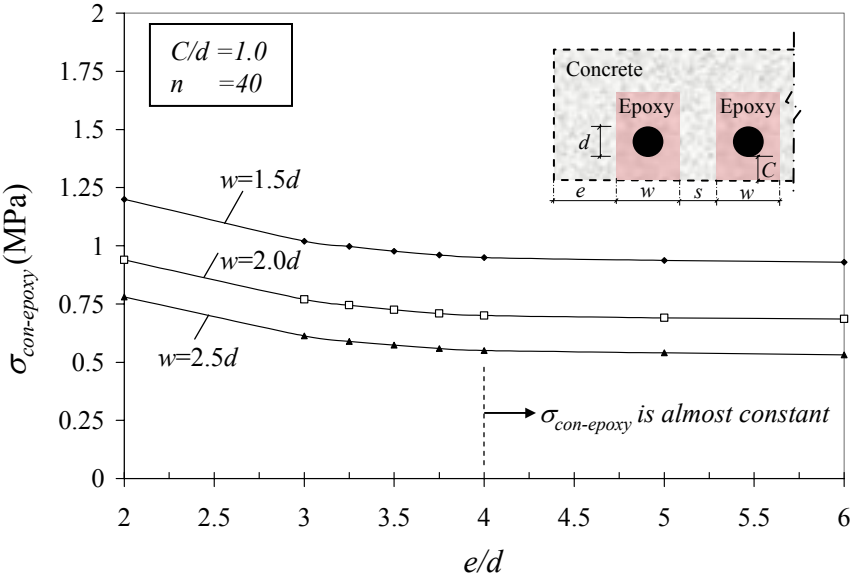

Fig. 12b Influence of edge distance on tensile stresses at the concrete-epoxy interface

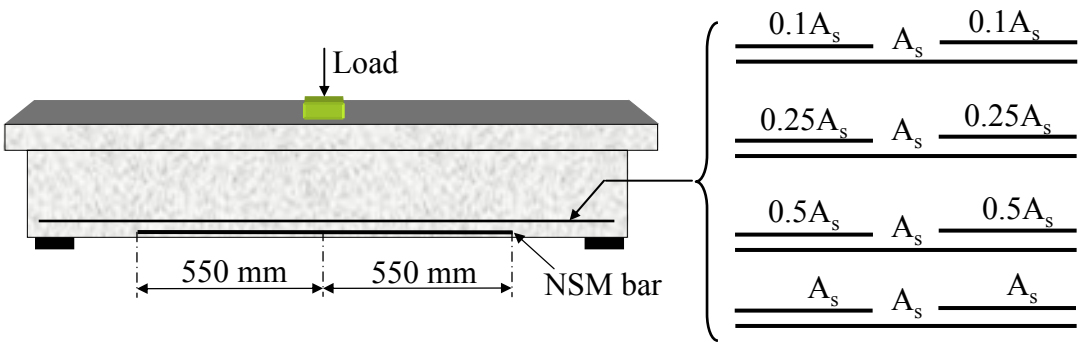

Fig. 13 Various configurations for the bottom steel reinforcement

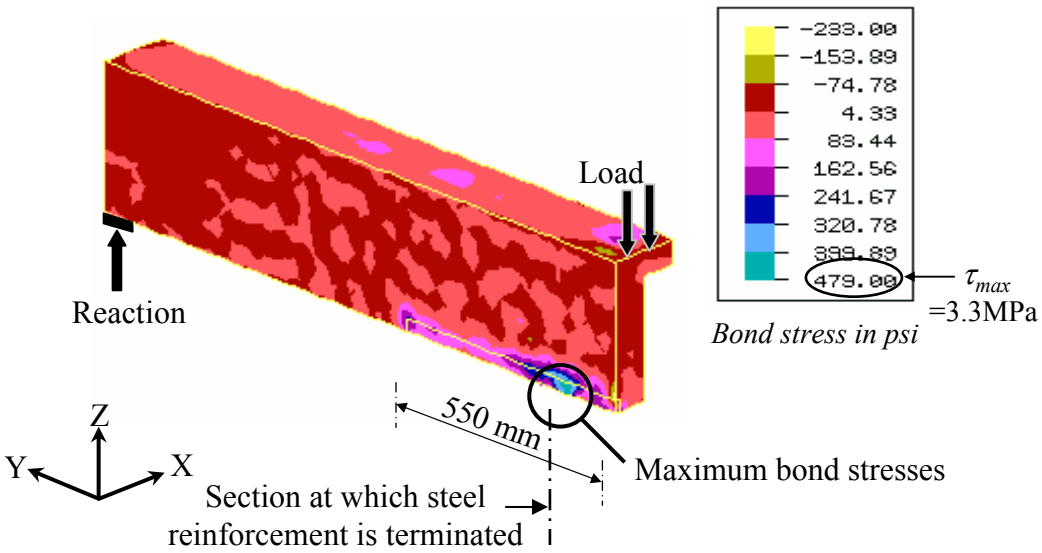

Fig. 14 Typical interfacial shear stress distribution at failure